



Regular Article

Structural aspects of magnetic softening in Fe-based metallic glass during annealing

J. Dai^a, Y.G. Wang^{a,*}, L. Yang^a, G.T. Xia^a, Q.S. Zeng^b, H.B. Lou^b

HPSTAR
334-2017

^a College of Materials Science and Technology, Nanjing University of Aeronautics and Astronautics, Nanjing 210016, PR China^b Center for High Pressure Science and Technology Advanced Research (HPSTAR), 1690 Cailun Road, Pudong, Shanghai 201203, PR China

ARTICLE INFO

Article history:

Received 1 August 2016

Accepted 6 September 2016

Available online 14 September 2016

Keywords:

Metallic glass

Annealing

Synchrotron radiation

Soft magnetic materials

ABSTRACT

Amorphous Fe₈₁Si₉B₁₀ melt-spun ribbons were annealed at various temperatures to relieve the internal stress. Magnetic studies manifest the occurrence of magnetic softening. The structure evolution of samples was then investigated by synchrotron radiation X-ray diffraction. It was found that, from short-range order to medium-range order, a positive and negative sign for volumetric thermal strain alternates upon heating and the amplitude of strain decays. Moreover, extending to outer shells, thermal strain seems less temperature-dependent in terms of the rate of increment. Magnetic softening in Fe₈₁Si₉B₁₀ metallic glasses upon annealing may result from the inhomogeneous thermal strains.

© 2016 Acta Materialia Inc. Published by Elsevier Ltd. All rights reserved.

The past several decades have witnessed the booming development of advanced materials. Metallic glasses, a new family of materials, possess unprecedented mechanical and physical properties. Unlike crystals, metallic glasses do possess short-range order (SRO) and medium-range order (MRO). The MRO is constructed by SRO through the sharing of vertices, edges, and faces [1]. Fe-based metallic glasses have been competitive with Silicon steel in terms of excellent soft magnetic properties such as high saturation magnetic flux density (B_s) and low coercivity (H_c) [2,3]. Recently, accelerating demands of Fe-based amorphous alloys have motivated researchers to concern more about structural essence behind the macroscopic properties [4,5]. Heat treatment as well as composition design is widely adopted to optimize the properties of Fe-based metallic glasses. Lately, atomic-level stress theory has been successfully applied to characterize the local structure and interpret the modifications of these physical properties [6–8].

Various low-temperature annealing methods are performed to relax the disordered structure in Fe-based metallic glasses so as to reduce the stress-induced magnetic anisotropy and concomitant coercivity. However, using synchrotron radiation X-ray diffraction, the underlying atomic-scale mechanisms of magnetic softening in Fe-based metallic glasses upon annealing are rarely investigated. In recent years, the thermal strain in metallic glasses exposed to a thermal loading has been calculated from the shift in positions of pair distribution function [9]. The intrinsic non-uniformity of the glass structure can give a non-uniform coefficient of thermal expansion [10]. Taghvaei et al. [11] investigated the

length-scale dependent thermal strain imposed by heating of Co₄₀Fe₂₂Ta₈B₃₀ glassy particles and found that thermal strain calculated for the first atomic shell is negative and then gradually becomes positive with increasing distance from an average atom. In contrast, according to Scudino et al. [9], a significant expansion (i.e. an increase in free volume) occurs in the SRO, whereas contraction (i.e. annihilation of free volume) during heating is observed in the MRO. These reports indicate that inhomogeneous thermal strain can take place for metallic glasses during annealing, i.e., that the positive or negative thermal strain occurs in the nearest atomic shell before changing its sign on medium-range length-scale. In our work, the magnetic and physical structures of as-quenched and isothermally annealed Fe₈₁Si₉B₁₀ glassy ribbons were investigated by Mössbauer spectroscopy and Synchrotron radiation X-ray diffraction. It was found that a positive and negative sign for the volumetric thermal strain ε alternates with increasing distance from an average atom upon heating (from SRO to MRO). This observation is obviously different from previous reports on inhomogeneous thermal strain during annealing.

The ingots of Fe₈₁Si₉B₁₀ were prepared by arc-melting a mixture of industry raw materials: Fe (99.9%), Si—Fe (Si: 99.586%, Fe: 0.27%), B—Fe (B:17.0%, Fe:83.0%) in an argon atmosphere. Using electromagnetic mixing, the alloy ingots were remelted four times in a Ti-gettered argon atmosphere to assure homogeneity. A single-roller melt spinning method in an argon atmosphere onto a copper wheel with a surface velocity of 40 m/s was adopted to produce amorphous ribbons. The ribbon width and thickness were 1.5 mm and 25 μ m, respectively. The as-quenched amorphous ribbons A₀ were isothermal annealed at 523, 543, 563 K for 480 s to get three independent glassy samples A₁, A₂, A₃, respectively, under the Ar flow and then cooled to room temperature

* Corresponding author.

E-mail address: yingang.wang@nuaa.edu.cn (Y.G. Wang).

in the furnace. Transmission Mössbauer spectra were collected at room temperature with a $^{57}\text{Co}(\text{Rh})$ source. The experimental spectra were fitted by NORMOS program. The coercivity H_c of the samples was determined from analysis of DC B–H loop tracer. The maximum magnetizing field of 8000 A/m was applied parallel to the longitudinal direction of ribbons. The structure of all samples was then tested by synchrotron radiation X-ray diffraction with a wavelength of 0.117418 Å by using beam line 11-IDC in the Advanced Photon Source of USA. A Mar345 image plate was used to record two dimensional diffraction data. Subsequently, the diffraction data were normalized by software PDFgetX2 [4] to get structure factors $S(Q)$ and corresponding pair distribution functions $G(r)$.

Since rapid-quenching generates complex residual stress, structural relaxation is performed by low-temperature annealing which is often accompanied by the process of magnetic softening for Fe-based metallic glasses. Mössbauer spectroscopy, as an efficient tool, is widely applied to characterize the stress-induced anisotropy in Fe-based metallic glasses. Room temperature Fe^{57} Mössbauer spectra of all specimens are illustrated in Fig. 1(a). Six broadened lines, typical of amorphous phases, can be observed in the patterns of as-quenched and isothermal annealed specimens, implying the existence of nonequivalent Fe sites. The six absorption lines have intensities determined by the angle θ between the directions of the γ rays and the local magnetization. It has been suggested that the intensity ratio of the second line relative to the third line can be used to monitor the direction of the easy axis of

magnetization in Fe-based amorphous alloys [12]. Thus, the intensity of the second line, relative to the third line, of the Mössbauer spectra can be given by

$$R = \frac{I_2}{I_3} = \frac{4\sin^2\theta}{1 + \cos^2\theta} \quad (1)$$

where θ is the angle between the γ rays and the local magnetization. B–H curves of as-quenched and annealed $\text{Fe}_{81}\text{Si}_9\text{B}_{10}$ alloy ribbons are shown in Fig. 1(b). The partial enlarged details of B–H curves are illustrated in the inset. The intensity ratio R of the second line relative to the third line in Mössbauer spectra and coercivity H_c as functions of the annealing temperature are depicted in Fig. 1(c). One can note that the value of R monotonically increases with the annealing temperature. The growth of R implies the ongoing increase in θ with an increase of annealing temperature. It means that the easy axis rotates towards the ribbon plane. Meanwhile, the coercivity H_c significantly decreases during annealing, which verifies the results from Mössbauer spectra. We believe that the relaxation of amorphous $\text{Fe}_{81}\text{Si}_9\text{B}_{10}$ alloy ribbons and concomitant magnetic softening occur in the annealing temperature range between 523 K and 563 K, according to previous reports [13,14]. However, atomic-scale structural mechanisms of magnetic softening in Fe-based metallic glasses upon temperature rise remain elusive. Therefore, it's worthwhile to investigate the structural changes during low-temperature annealing in more detail.

Room temperature structure factors $S(Q)$ of as-quenched and annealed ribbons are illustrated in Fig. 2(a). As can be seen, the diffuse scattering patterns remain unchanged for ribbons annealed at various temperatures, indicating the preservation of amorphous nature during low-temperature annealing. Pronounced oscillations proceed up to $Q = 16 \text{ \AA}^{-1}$. Variations in positions q_1 and q_2 of the first and second diffuse maxima with annealing temperature are depicted in Fig. 2(b). The peak positions q_1 and q_2 were obtained by fitting the top of the peak using a pseudo-Voigt function. It has been known that changes in positions of diffuse maxima of $S(Q)$ indicate atomic-scale structural evolution. Little change is observed for q_1 , while there is an obvious reduction in q_2 , indicating the occurrence of inhomogeneous structural changes in different atomic shells. It is therefore anticipated that

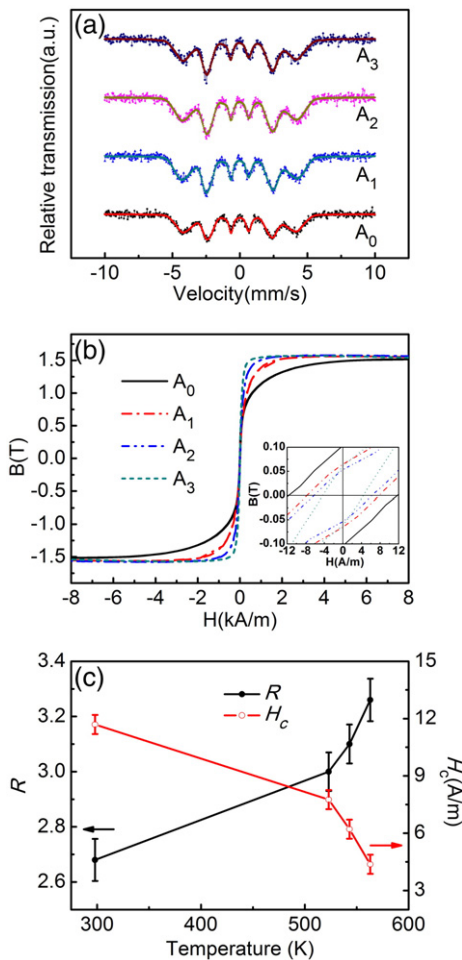


Fig. 1. (a) Room temperature Fe^{57} Mössbauer spectra of melt-spun (A_0) and annealed (A_1 , A_2 , & A_3) ribbons together with their fits. (b) B–H curves of as-quenched and annealed ribbons. (c) The intensity ratio R of the second line relative to the third line in Mössbauer spectra and coercivity H_c as functions of annealing temperature.

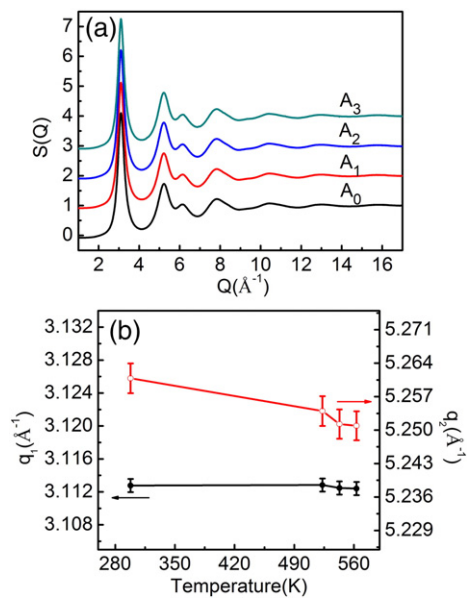


Fig. 2. (a) Structure factors $S(Q)$ of $\text{Fe}_{81}\text{Si}_9\text{B}_{10}$ alloy melt-spun (A_0) and annealed (A_1 , A_2 , & A_3) ribbons. (b) The first and second diffuse maxima q_1 and q_2 as functions of annealing temperature.

no-uniform atomic-scale structural changes appear in different atomic shells upon temperature rise.

To seek the possible atomic-scale structural transformations from SRO to MRO upon annealing, a further more detailed study of annealing-induced structural evolution was conducted in the real space. Fig. 3 shows pair distribution function $G(r)$ of as-quenched and annealed ribbons. The partial enlarged details of $G(r)$ around the first peak position are illustrated in the inset. It can be observed that temperature rise induces variations in the position of $G(r)$ peaks in the first coordination shell and the peak position moves to large value of r . This indicates the variation in atomic-level stress as concluded by Egami et al. [15]. However, the shift in the first peak position of $G(r)$ is not significant and needs to be quantified. According to $G(r)$ patterns in Fig. 3, positions of $G(r)$ peaks can be obtained by Gaussian fits. According to the related work [9,11], the volumetric thermal strain ε can thus be obtained by calculating shifts in positions of $G(r)$ peaks as

$$\varepsilon = \left(\frac{r}{r_0}\right)^3 - 1, \quad (1)$$

where r_0 and r are positions of $G(r)$ peaks of as-quenched and annealed ribbons, respectively. Fig. 4(a) shows the volumetric thermal strains ε of $\text{Fe}_{81}\text{Si}_9\text{B}_{10}$ amorphous ribbons at various annealing temperatures determined from $G(r)$ peaks. It is observed that for all annealed ribbons a positive and negative sign for the volumetric thermal strain alternates with the increase of r and the amplitude of ε gradually decays from SRO to MRO length scale. Moreover, significant oscillation of ε occurs in the first six coordination shells, indicating the alternation of tensile stress and compressive stress sites in the first six atomic shells. The thermal strains for atoms in MRO present on a length scale larger than $r = 10 \text{ \AA}$ slightly fluctuate, and the negative ε imply that compressive stress is predominant on this length scale. Our results suggest that atomic-level and cluster-level structural changes take place during low-temperature annealing. The presence of such positive and negative thermal strain sites results in the relaxation of internal stress in $\text{Fe}_{81}\text{Si}_9\text{B}_{10}$ metallic glass. It has been pointed out that structure change on short-range length scale can develop in certain atomic clusters during annealing and the interconnectivity between clusters generates an increase in the elastic modulus and strength [16]. In our work, it is possible that atomic-scale thermal expansion occurs in the nearest-neighbor distance within a cluster. One the one hand, different atomic environment for centered atom makes it possible to affect the nearest atoms, and vice versa. One the other hand, the transformation of MRO is determined by the interactions between clusters. We believe that thermal expansion may initiate in the first atomic shell and somehow transmits the applied thermal loading to other coordination shells through the connection of clusters. This may interpret the deformation behaviors of first six atomic shells and thus changes of the first six $G(r)$ peaks. $G(r)$

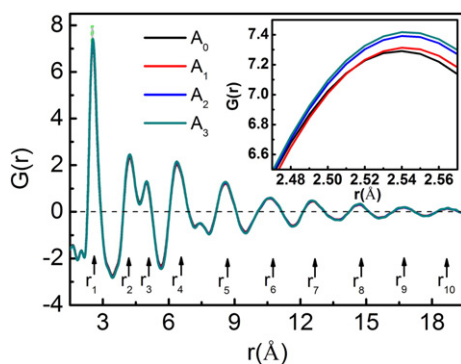


Fig. 3. Pair distribution functions $G(r)$ of melt-spun (A_0) and annealed (A_1 , A_2 , & A_3) $\text{Fe}_{81}\text{Si}_9\text{B}_{10}$ alloy ribbons. Inset: $G(r)$ curves at the first peak position.

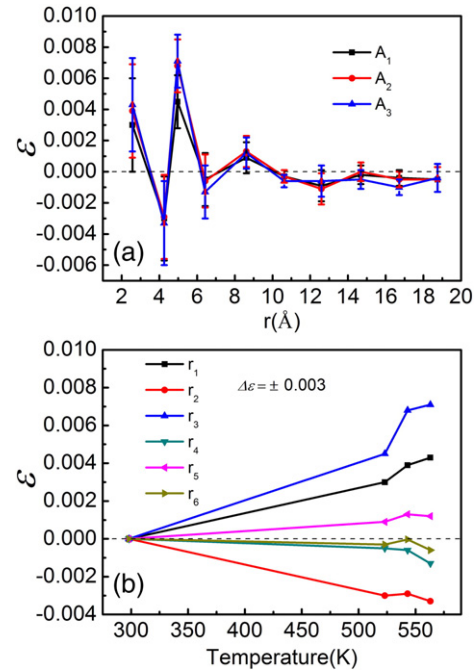


Fig. 4. (a) Volumetric thermal strains ε of amorphous ribbons annealed at various temperatures determined from $G(r)$ peaks. (b) Volumetric thermal strains ε determined from the first six peaks of $G(r)$ individually as functions of annealing temperature.

results reveal that the degree of order decreases with increasing of r . The MRO as well as SRO probably plays an important role in the deformation of amorphous alloys induced by annealing. However, it is unclear about the details of those connection mechanisms, and much future work needs to be done.

The volumetric thermal strain ε for the first six peaks of $G(r)$ as functions of annealing temperature was depicted in Fig. 4(b). It can be seen that the volumetric thermal strains ε monotonically increase with annealing temperature. The alternation of tensile and compressive strains proceeds in the first six nearest-neighbor atomic shells. Furthermore, the rate of increment of thermal strain becomes less temperature dependent with the increase of distance from the average atom. Therefore, the distribution of thermal strain within ribbons is both annealing temperature and length scale dependent. Consistent with the expectation from Mössbauer spectroscopy, stress release goes on with an increase in annealing temperature and $\text{Fe}_{81}\text{Si}_9\text{B}_{10}$ amorphous ribbons are expected to be more relaxed.

In conclusion, we investigated local structure changes on annealing in $\text{Fe}_{81}\text{Si}_9\text{B}_{10}$ amorphous ribbons by Mössbauer spectroscopy and synchrotron radiation X-ray diffraction. The magnetic softening with the increase of annealing temperature originates from the stress relief upon annealing, where the inhomogeneous thermal strain occurs. We observed that a positive and negative sign for the volumetric thermal strain ε alternates from SRO to MRO, and ε gradually decays before it reaches to almost a constant value on medium-range length scale. Furthermore, ε monotonically increases with annealing temperature and seems less temperature-dependent extending to outer atomic shells in terms of rate of increment. The inhomogeneous thermal strains upon temperature rise contribute to rotation of easy magnetization direction and the concomitant reduction in coercivity of $\text{Fe}_{81}\text{Si}_9\text{B}_{10}$ alloy ribbons.

We thank the Advanced Photon Source in USA for the use of the advanced synchrotron radiation facilities. This work is supported by National Nature Science Foundation of China (No. 51571115), Joint Innovation Foundation of Industry and University of Jiangsu Province (No. BY2013003-01) and a Project Funded by the Priority Academic Program Development of Jiangsu Higher Education Institutions.

References

- [1] D. Ma, A.D. Stoica, X.L. Wang, *Nat. Mater.* 8 (2009) 30–34.
- [2] A. Urata, M. Yamaki, K. Satake, H. Matsumoto, A. Makino, *J. Appl. Phys.* 113 (2013) 17A311.
- [3] P. Sharma, X. Zhang, Y. Zhang, A. Makino, *J. Appl. Phys.* 115 (2014) 17 A340.
- [4] Q. Yu, X.D. Wang, H.B. Lou, Q.P. Cao, J.Z. Jiang, *Acta Mater.* 102 (2016) 116–124.
- [5] Y.C. Wang, A. Takeuchi, A. Makino, Y.Y. Liang, Y. Kawazoe, *J. Appl. Phys.* 115 (2014) 173910.
- [6] A.H. Taghvaei, M. Stoica, I. Kaban, J. Bednarčík, J. Eckert, *J. Appl. Phys.* 116 (2014) 054904.
- [7] Y.M. Wang, M. Zhang, L. Liu, *Scr. Mater.* 102 (2015) 67–70.
- [8] J. Ding, Y.Q. Cheng, *Appl. Phys. Lett.* 104 (2014) 051903.
- [9] S. Scudino, M. Stoica, I. Kaban, K.G. Prashanth, G.B.M. Vaughan, J. Eckert, *J. Alloys Compd.* 639 (2015) 465–469.
- [10] S.V. Ketov, Y.H. Sun, S. Nachum, Z. Lu, A. Checchi, A.R. Beraldin, H.Y. Bai, W.H. Wang, D.V. Louzguine-Luzgin, M.A. Carpenter, A.L. Greer, *Nature* 524 (2015) 200.
- [11] A.H. Taghvaei, H.S. Shahabi, J. Bednarčík, J. Eckert, *J. Appl. Phys.* 117 (2015) 044902.
- [12] J.V. Kasiuk, J.A. Fedotova, J. Przewoznik, J. Zukrowski, M. Sikora, C. Kapusta, A. Grce, M. Milosavljević, *J. Appl. Phys.* 116 (2014) 044301.
- [13] T. Pradell, N. Clavaguera, J. Zhu, M.T. Clavaguera-Mora, *J. Phys. Condens. Matter* 7 (1995) 4129–4143.
- [14] M. Sorescu, E.T. Knobbe, *Phys. Rev. B* 49 (1994) 3253–3265.
- [15] T. Egami, *Prog. Mater. Sci.* 56 (2011) 637–653.
- [16] J. Zemp, M. Celino, B. Schönfeld, J.F. Löffler, *Phys. Rev. Lett.* 115 (2015) 165501.